Molecular Therapy
Original Article

sEVs from tonsil-derived mesenchymal stromal cells alleviate activation of hepatic stellate cells and liver fibrosis through miR-486-5p

Jieun Kim,[1,5] Chanbin Lee,[1,5] Yongbo Shin,[1,5] Sihyung Wang,[1] Jinsol Han,[1] Minju Kim,[1] Ji Min Kim,[2] Sung-Chan Shin,[3] Byung-Joo Lee,[3] Tae-Jin Kim,[1,4] and Youngmi Jung[1,4]

[1]Department of Integrated Biological Science, College of Natural Science, Pusan National University, Pusan 46241, Republic of Korea; [2]Pusan National University Medical Research Institute, Pusan National University School of Medicine, Pusan 49241, Republic of Korea; [3]Department of Otorhinolaryngology-Head and Neck Surgery, College of Medicine, Pusan National University and Medical Research Institute, Pusan National University Hospital, Pusan 49241, Republic of Korea; [4]Department of Biological Sciences, College of Natural Science, Pusan National University, Pusan 46241, Republic of Korea

Mesenchymal stromal cells (MSCs) are considered as a promising therapeutic tool for liver fibrosis, a main feature of chronic liver disease. Because small extracellular vesicles (sEVs) harboring a variety of proteins and RNAs are known to have similar functions with their derived cells, MSC-derived sEVs carry out the regenerative capacities of MSCs. Human tonsil-derived MSCs (T-MSCs) are reported as a novel source of MSCs, but their effects on liver fibrosis remain unclear. In the present study, we investigated the effects of T-MSC-derived sEVs on liver fibrosis. The expression of profibrotic genes decreased in human primary hepatic stellate cells (pHSCs) co-cultured with T-MSCs. Treatment of T-MSC-sEVs inactivated human and mouse pHSCs. Administration of T-MSC-sEVs ameliorated hepatic injuries and fibrosis in chronically damaged liver induced by carbon tetrachloride (CCl_4). miR-486-5p highly enriched in T-MSC-sEVs targeting the hedgehog receptor, smoothened (Smo), was upregulated, whereas Smo and Gli2, the hedgehog target gene, were downregulated in pHSCs and liver tissues treated with T-MSC-sEVs or miR-486-5p mimic, indicating that sEV-miR-486 inactivates HSCs by suppressing hedgehog signaling. Our results showed that T-MSCs attenuate HSC activation and liver fibrosis by delivering sEVs, and miR-486 in the sEVs inactivates hedgehog signaling, suggesting that T-MSCs and their sEVs are novel anti-fibrotic therapeutics for treating chronic liver disease.

INTRODUCTION

Chronic liver disease occurs in response to persistent long-term liver injury, such as viral hepatitis, obesity, or alcohol abuse.[1] Although the etiologies of liver diseases may vary, a common pathological feature of most chronic liver diseases is liver fibrosis, which is characterized by the progressive replacement of functional hepatic tissue with extracellular matrix (ECM).[1] Excessive accumulation of ECM perturbs the normal function of the liver and eventually leads to the end stage of cirrhosis or liver cancer. Hepatic stellate cells (HSCs) are a key fibrogenic cell type that contributes to liver fibrosis.[2] Liver fibrogenesis is initiated by HSC activation. In normal liver, quiescent HSCs (Q-HSCs) maintain a nonproliferative phenotype and are responsible for the storage of vitamin A/retinoic acid. Upon liver injury, HSCs become activated and transdifferentiate into myofibroblastic HSCs, which are proliferative and produce ECM, such as collagens, in the damaged liver.[1,2] Hence, regulating HSC activation could be a potential therapeutic strategy for antifibrotic therapy.

Mesenchymal stromal cells (MSCs) are multipotent adult stem cells with the ability to self-renew and differentiate into multiple cell lineages.[3] Since MSCs possess considerable tissue regenerative effects and immunomodulatory properties, the therapeutic effects of MSC transplantation have been widely studied in clinical and experimental research, including in chronic liver disease. Many studies have reported that the therapeutic effects of MSCs against liver fibrosis/cirrhosis are related to their capacity to undergo hepatocyte-like differentiation, immunomodulatory properties, and secretory paracrine actions.[4–10] MSCs have been successfully identified and isolated from adult tissues such as bone marrow, adipose, placenta, amniotic fluid, and umbilical cord blood tissues.[3] Recently, palatine tonsils, commonly called tonsils, have been considered a novel promising source of MSCs.[11] Human tonsils are lymphoepithelial tissues that act as immune organs until puberty and undergo atrophy during aging. Tonsil-derived MSCs (T-MSCs) can be easily obtained from surgically removed tonsil tissues after tonsillectomy to treat chronic tonsillitis or tonsillar hypertrophy. Similar to other MSCs, such as bone marrow-derived MSCs (BM-MSCs) or adipose tissue-derived MSCs (A-MSCs), T-MSCs exhibit self-renewal capacity, multilineage differentiation properties, and immunosuppressive characteristics.[11–13] In addition, growing evidence

Received 12 June 2020; accepted 15 December 2020;
https://doi.org/10.1016/j.ymthe.2020.12.025.

[5]These authors contributed equally

Correspondence: Youngmi Jung, PhD, Department of Biological Sciences, College of Natural Science, Pusan National University, 63-2 Pusandaehak-ro, Keumjeong-gu, Pusan 46241, Republic of Korea.
E-mail: y.jung@pusan.ac.kr

has revealed the therapeutic benefits of T-MSCs in various diseases, such as allergic rhinitis, peripheral nerve injury, skin wound lesions, and liver fibrosis.[14–17] It has been reported that infusion of T-MSCs ameliorates carbon tetrachloride (CCl_4)-induced acute liver damage and fibrosis in mice by differentiating hepatocyte-like cells or promoting autophagic flux.[17] The same group has also shown that T-MSC-conditioned medium (CM) relieves CCl_4-induced liver fibrosis by decreasing hepatic inflammation.[18] These studies suggest the therapeutic potential of T-MSCs for treating liver disease. However, it remains unclear whether and how T-MSCs influence HSC activation.

Small extracellular vesicles (sEVs) with a diameter around 30–150 nm are secreted by all cell types and possess similar properties to their parental cells.[19,20] Since sEVs including exosomes carry a variety of cargoes, including proteins, mRNAs, and small noncoding RNAs, they have emerged as crucial mediators of intercellular communication and modulators of cellular activities in recipient cells.[21] Because MSCs also produce and secrete sEVs, it has been proposed that the regenerative ability of MSCs is mediated by sEVs and that their sEVs have a therapeutic potential similar to that of MSCs.[22,23] The therapeutic efficacy of MSC-derived sEVs has been reported in several disease models, such as autoimmune disease, cardiovascular disease, and liver disease.[24–26] Feng et al.[26] demonstrated that MSC-derived exosomes containing microRNA (miRNA or miR)-22 reduced infarct size and cardiac fibrosis by inhibiting apoptosis in mice with myocardial infarction. In a rat liver fibrotic model, miR-125b contained in exosomes derived from chorionic plate-derived MSCs (CP-MSCs) ameliorated hepatic fibrosis by suppressing hedgehog (Hh) signaling, which is an essential regulator in liver fibrosis.[25] These findings suggest that sEVs and their cargoes, mainly miRNAs, play important roles in MSC-mediated tissue repair and regeneration.

Given that sEVs mediate the regenerative abilities of MSCs and T-MSCs have therapeutic potential in liver diseases, we hypothesized that sEVs derived from T-MSCs might influence liver fibrosis. To prove our hypothesis, we investigated the effects of T-MSCs and T-MSC-originated sEVs in HSCs and chronically damaged liver. sEV-miRNAs involved in the action of T-MSC-sEVs were also examined in the current studies.

RESULTS

T-MSCs promote inactivation of HSCs

To investigate the effect of T-MSCs on activated HSCs, the human activated HSC line LX2 was cultured in T-MSC-CM for 2 days (T-MSC-CM group). LX2 cells cultured in normal culture media were used for the control group (CON group). The RNA levels of HSC activation markers, including transforming growth factor-β (*TGF-β*), α-smooth muscle actin (*α-SMA*), collagen type 1 α 1 chain (*COL1α1*), *VIMENTIN*, and connective tissue growth factor (*CTGF*), decreased significantly in the T-MSC-CM group compared with the CON group during culture (Figure S1A). However, the expression of glial fibrillary acidic protein (*GFAP*), a marker of Q-HSCs, was significantly increased in the T-MSC-CM group compared with the CON group. Western blot analysis confirmed the RNA data by showing lower expression of TGF-β, α-SMA, and VIMENTIN and higher expression of GFAP in the T-MSC-CM group than in the CON group (Figure S1B). After confirming the effect of T-MSCs on HSC activation, we further assessed the direct interactions between T-MSCs and human primary HSCs (pHSCs), which were already activated, using a coculture system. qRT-PCR showed that the levels of the HSC activation markers *TGF-β*, *α-SMA*, *COL1α1*, *VIMENTIN*, *CTGF*, and tissue inhibitor of metalloproteinase 1 (*TIMP1*) were significantly decreased and that the HSC inactivation marker *GFAP* was elevated in pHSCs cultured with T-MSCs compared with mono-cultured cells (Figure 1A). In addition, the protein levels of TGF-β, VIMENTIN, and α-SMA decreased, whereas that of GFAP increased in the coculture group compared with the mono-culture group (Figure 1B). These results indicate that T-MSCs influence HSC activation.

T-MSC-derived sEVs inhibit the activation of HSCs

Because MSCs are known to release sEVs for intercellular communication or to mediate the paracrine activity of MSCs,[23] we examined whether sEVs secreted from T-MSCs affected HSC activation. sEVs were isolated from culture media of T-MSCs that were incubated for 48 h in sEV-depleted media. The size of the isolated sEVs mostly ranged from 50 to 290 nm, as assessed by the dynamic light scattering (DLS) system (Figure 2A). Transmission electron microscopy (TEM) analysis showed that the isolated sEVs had a cup-shaped morphology, which is a common morphological feature of sEVs, and their size was determined to be 50–100 nm in diameter (Figure 2B). Western blot analysis additionally confirmed the isolated sEVs by showing the presence of the sEV markers CD63, CD9, and CD81 and the absence of calreticulin, which is an endoplasmic reticulum-resident protein and a negative marker for sEVs (Figure 2C). After verifying that sEVs excluding other extracellular vesicles were well isolated from cultured media of T-MSCs, human activated pHSCs were treated with T-MSC-derived sEVs at different concentrations (0, 1, 10, or 100 μg/mL) for 2 days to assess the effect of T-MSC-derived sEVs on activated HSCs. Vehicle-treated pHSCs were used for the CON group. Compared to that in vehicle-treated pHSCs, the expression of *TGF-β*, *α-SMA*, *VIMENTIN*, and *CTGF* was significantly reduced in pHSCs at day 2 after treatment with 100 μg/mL sEVs, as assessed by qRT-PCR (Figure 3A). Their protein levels also showed a notable decrease in pHSCs exposed to 100 μg/mL sEVs at day 2 compared with other groups (Figure 3B). To investigate the uptake of T-MSC-derived sEVs, these cells were cultured in medium and exposed to 100 μg/mL sEVs labeled with PKH67 for 2 and 4 h. The co-localization of the labeled sEVs within the cell by fluorescence and confocal microscopy demonstrated successful uptake (Figure 3C). These results indicate that T-MSC-derived sEVs suppressed HSC activation.

sEVs derived from T-MSCs reduce hepatic damage and collagen deposition in the liver

Before examining the *in vivo* effects of human T-MSC-derived sEVs on an experimental fibrotic murine model, we assessed their action in primary activated HSCs isolated from mice with chronic CCl_4-induced liver injury. Cells treated with sEVs for 2 days had

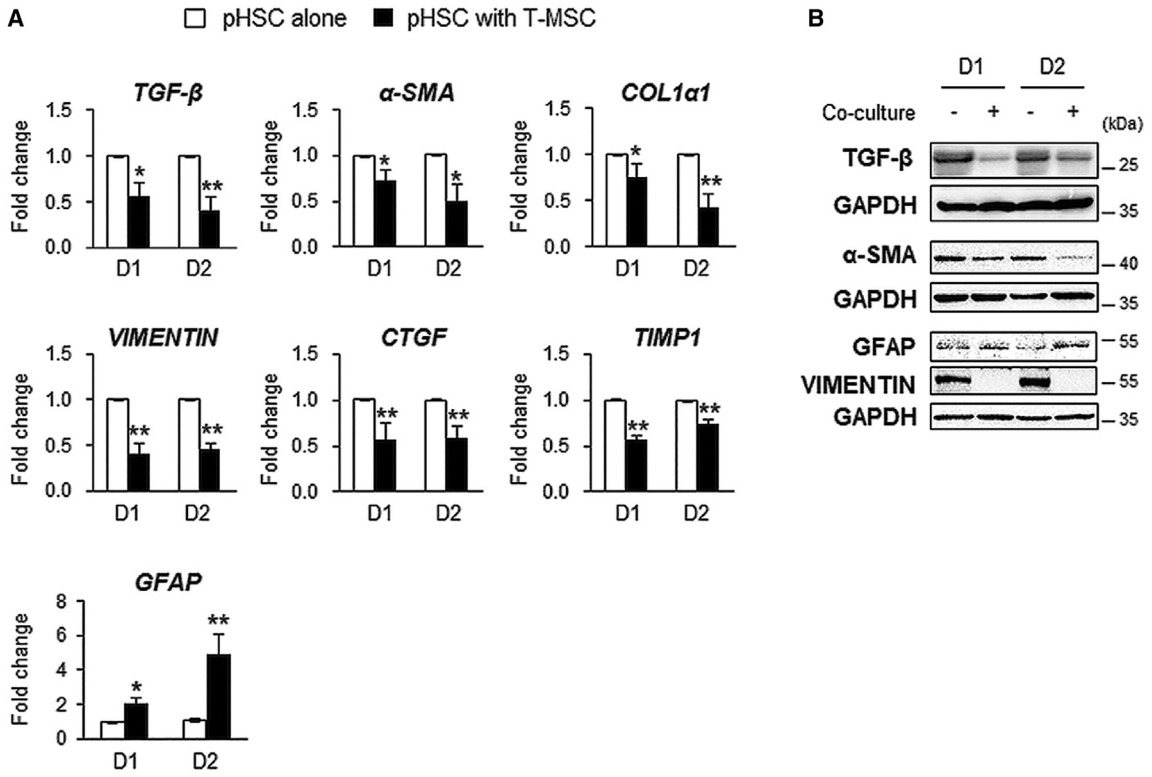

Figure 1. T-MSCs inactivate human pHSCs

(A) qRT-PCR analysis for *TGF-β*, *α-SMA*, *COL1α1*, *VIMENTIN*, *CTGF*, *TIMP1*, and *GFAP* in human pHSCs cultured alone (pHSC alone) or co-cultured with T-MSCs (pHSC with T-MSC) for 1 day (D1) or 2 days (D2). Data are presented as mean ± SEM of experiments performed in triplicate (unpaired two-sample Student's t test; *$p < 0.05$, **$p < 0.005$ versus own control). (B) Western blot analysis for TGF-β (25 kDa), VIMENTIN (57 kDa), α-SMA (42 kDa), GFAP (50 kDa) and GAPDH (36 kDa) in these cells. GAPDH was used as an internal control. Immunoblots shown represent one of three independent experiments with similar results.

significantly lower expression levels of *Tgf-β*, *α-Sma*, *Vimentin*, *Ctgf*, and *Timp1* than vehicle-treated cells (Figure 4A). To investigate the functional effects of T-MSC-derived sEVs on chronic hepatic fibrosis, we injected sEVs into mice with CCl_4-induced liver fibrosis. Mice were intraperitoneally treated with CCl_4 or corn oil (CON group) for 3 weeks and then injected with T-MSC-derived sEVs (CCl_4+sEV group) or vehicle (CCl_4+phosphate-buffered saline [PBS] group) via the intravenous route three times for 2 weeks. Mice were continuously injected with CCl_4 for an additional 2 weeks and then sacrificed (Figure S2A). For the CON groups, mice were intraperitoneally injected with CCl_4 (CCl_4 group) or corn oil (CON group) for 5 weeks. In the examination of livers of mice from the CON, CON+PBS, and CON+sEV groups, no significant difference among these CON groups was detected, as assessed by hematoxylin and eosin (H&E) staining, Sirius red staining, liver weight (LW)-to-body weight (BW) ratio, and serum alanine aminotransferase/aspartate aminotransferase (ALT/AST) levels (Figures S2B and S2C). In addition, the protein levels of Tgf-β, α-Sma, Vimentin, and Col1α1 were very low or hardly detected in these mice (Figure S2D). After confirming that sEVs themselves rarely affect healthy livers, we examined their effects in mouse fibrotic liver. The CON+PBS group was also used as a CON group in this analysis. H&E staining showed severe hepatic injuries with distorted morphological structures in CCl_4-treated mice with or without PBS compared with the corn oil-treated mice with PBS. However, these abnormal morphological changes were noticeably ameliorated in the livers of CCl_4-treated mice injected with sEVs compared with the other CCl_4-treated groups (Figure 4B). Although the LW/BW ratios were similar among the four groups (Table S2), the serum levels of ALT and AST decreased in the CCl_4+sEV group compared with the CCl_4 and CCl_4+PBS groups (Figure 4C). The RNA level of glucose-6-phosphatase (*G6pc*), which represents normal liver function, was reduced in the CCl_4 and CCl_4+PBS groups, whereas its expression in the CCl_4+sEV group was restored to the nearly basal levels of the CON group (Figure 4D).

Because the sEV-treated group had improved liver morphology and function *in vivo* and these sEVs suppressed HSC activation *in vitro* (Figure 4), we examined whether the level of fibrosis was attenuated in these mice. The expression of the fibrotic markers *Tgf-β*, *α-Sma*, *Vimentin*, and *Ctgf* was significantly reduced in the CCl_4+sEV group compared with the other CCl_4 groups, as assessed by qRT-PCR (Figure 5A). The protein levels of these markers were also significantly decreased in the livers of the CCl_4+sEV group compared with the CCl_4 and CCl_4+PBS groups (Figures 5B and 5C). Sirius red staining

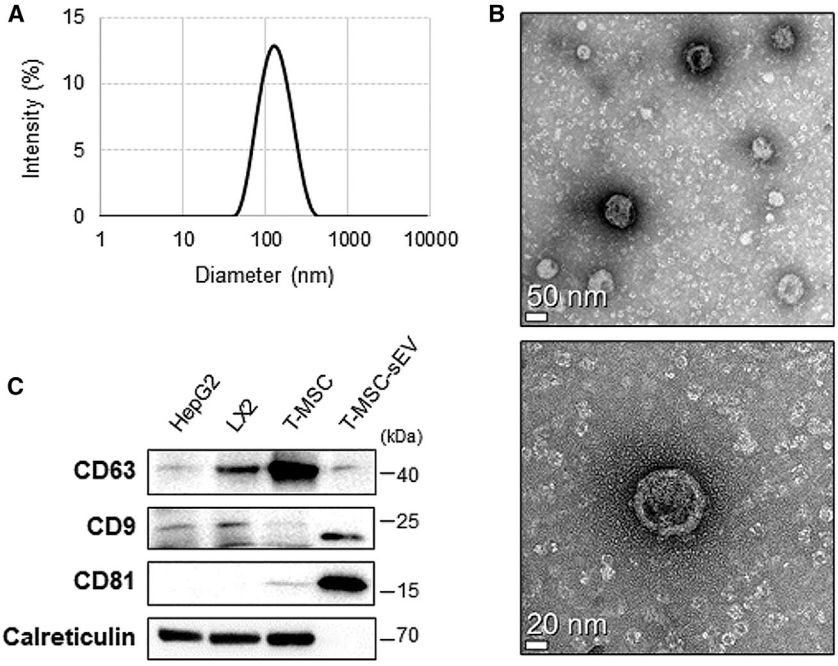

Figure 2. Characterization of sEVs isolated from T-MSCs

(A) The size distribution of sEVs isolated from T-MSCs was measured by dynamic light scattering. (B) Representative microscopic images were obtained from TEM analysis for detecting isolated sEVs. (C) Western blot analysis of sEV surface markers CD63 (45 kDa), CD9 (25 kDa), and CD81 (17 kDa) and sEVs negative marker CALRETICULIN (64 kDa) in HepG2, LX2, T-MSCs, and sEVs isolated from T-MSCs (T-MSC-sEV). Immunoblots shown represent one of three independent experiments with similar results.

revealed that excessive collagen fibrils were deposited in the livers of the CCl_4 and CCl_4+PBS groups compared with the livers of the CON+PBS group, while collagen accumulation was remarkably ameliorated in the livers of the CCl_4+sEV group (Figure 5D, top panel). Immunohistochemistry (IHC) for α-SMA, a marker for activated HSCs,[27,28] clearly presented that α-SMA-positive cells accumulated and formed fibrous septa in the liver tissues from CCl_4-treated mice with or without PBS, whereas these cells were less evident in the livers of sEV-treated mice with CCl_4 exposure (Figure 5D, bottom panel). In the CON groups, these cells were rarely detected (Figure S2B, bottom panel). The hydroxyproline assay also confirmed that hydroxyproline contents in the livers were considerably lower in the CCl_4+sEV group than in the other CCl_4 groups (Figure 5E).

Taken together, these findings suggest that T-MSC-derived sEVs alleviated liver damage and fibrosis.

sEV-miR-486-5p derived from T-MSCs inactivates HSCs by suppressing the expression of its target SMO

miRNAs are among the sEV cargoes, and miRNAs transferred by sEVs into target cells impact cell behaviors by regulating the expression of target genes.[19] Because sEVs derived from T-MSCs influenced HSC activation, we assessed which miRNAs contained in sEVs regulated HSC activation. Four candidate miRNAs, miR-185-5p, miR-125b-5p, miR-486-5p, and miR-130a-3p, were selected based on previous reports, including a microarray analysis (GEO: GSE77272) and small RNA sequencing analysis, because these four miRNAs are abundantly expressed in T-MSCs.[13,29] In addition, the potential link between four miRNAs and fibrosis was found in independent previous studies.[25,30–32] The levels of *miR-185-5p*, *miR-125b-5p*, *miR-486-5p*, and *miR-130a-3p* were higher in T-MSC-derived sEVs than in LX2 cells, pHSCs, or normal human liver tissues, and among them, *miR-486-5p* was significantly enriched in these sEVs, suggesting the possibility that miR-486-5p might be involved in modulating HSC activation (Figure 6A). Bioinformatics analysis using miRWalk predicted smoothened (SMO), a receptor for the Hh pathway, as a putative target of miR-486-5p (Figure 6B), and the luciferase reporter assay revealed that miR-486-5p directly bound to the 3′ untranslated region (UTR) of *SMO* mRNA in both HepG2 and LX2 cells (Figure 6C). To examine whether miR-486-5p impacted HSC activation, human activated pHSCs were transfected with miR-486-5p mimic or scrambled (Scr)-miR. Although *miR-486-5p* was rarely expressed in activated pHSCs (Figure 6A), its expression was greatly elevated in miR-486-5p-transfected pHSCs; sequentially, the levels of the miR-486-5p-targeted *SMO* and GLI-Kruppel family member GLI2 (*GLI2*), an Hh transcription factor, were significantly decreased in these cells compared with those in Scr-transfected cells (Figure 7A). In addition, the profibrotic markers *TGF-β*, *α-SMA*, *VIMENTIN*, and *CTGF* were downregulated in pHSCs transfected with miR-486-5p compared with Scr-miR. Western blot assays confirmed the RNA data by showing reduction in SMO, GLI2, and profibrotic markers in pHSCs transfected with miR-486-5p (Figures 7B and 7C). These results suggest that miR-486-5p inhibits HSC activation by directly targeting *SMO*.

To determine whether T-MSC-derived sEVs transfer miR-486-5p to HSCs and whether the transferred miR-478-5p suppresses SMO expression in our experimental system, we examined the levels of miR-486-5p, SMO, and GLI2 in pHSCs treated with sEVs (Figure 3) and in the livers of the CCl_4+sEV group (Figures 4 and 5). The expression of *miR-486-5p* significantly increased and the amounts of *SMO* and GLI2 decreased in sEV-treated pHSCs compared with vehicle-treated cells, as assessed by qRT-PCR and western blot assays (Figures 8A and 8B). In line with the *in vitro* data, the level of *miR-486-5p* was significantly higher in the livers of the CCl_4+sEV group than in the livers of the other three groups, that is, CON+PBS, CCl_4, and CCl_4+PBS (Figure 8C). For *in situ* PCR analysis for miR-486-5p in these mice, miR-486-5p-expressing cells (blue/violet-colored) were

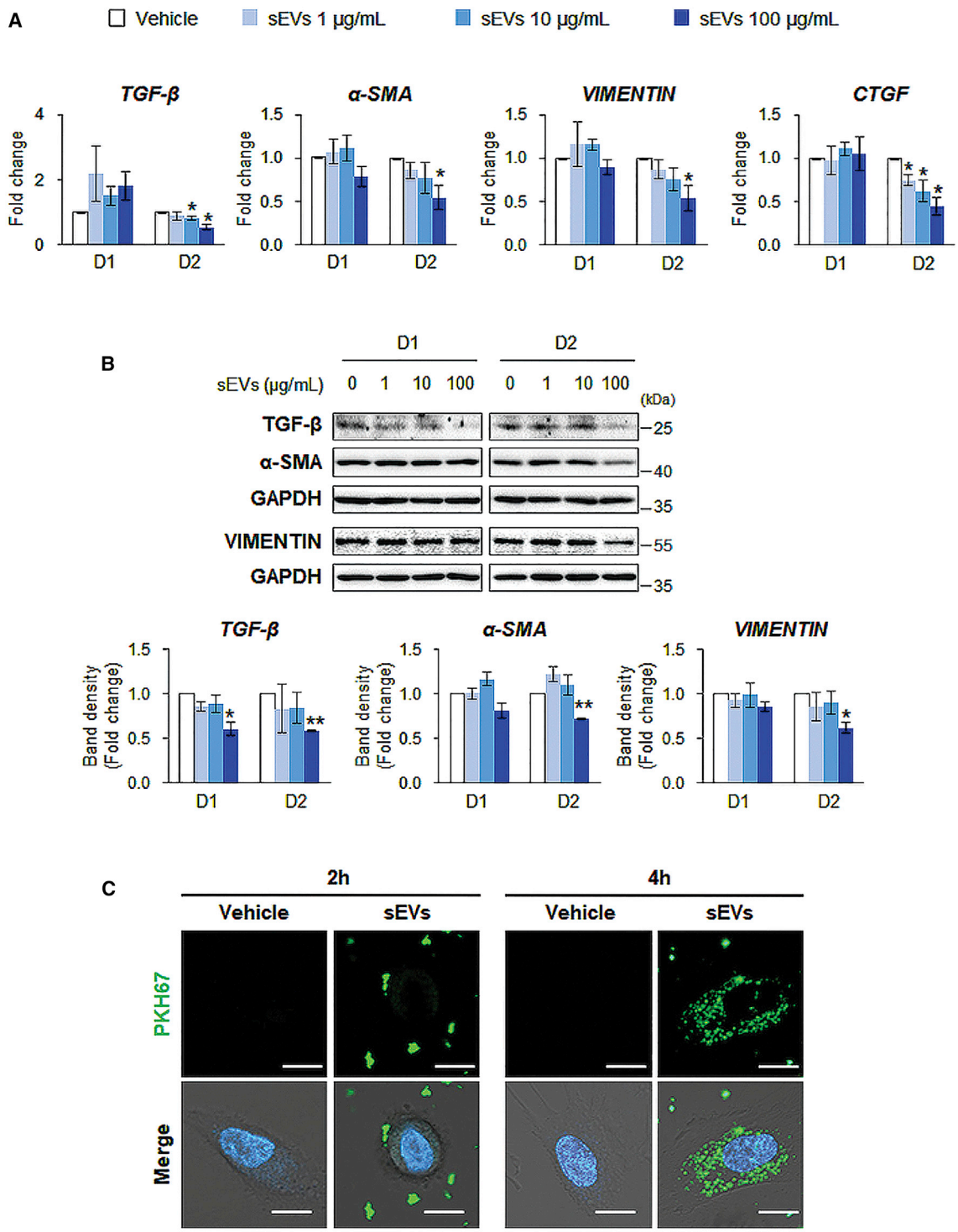

Figure 3. Treatment of T-MSC-derived sEVs downregulates profibrotic genes in human pHSCs

(A) qRT-PCR analysis for *TGF-β*, *α-SMA*, *VIMENTIN*, and *CTGF* in pHSCs treated with vehicles (PBS) or T-MSC-sEV (1, 10, and 100 µg/mL) for 1 day (D1) or 2 days (D2). Data are presented as mean ± SEM of experiments performed in triplicate (unpaired two-sample Student's t test; *p < 0.05 versus own control). (B) Western blot and cumulative densitometry analyses of TGF-β (25 kDa), α-SMA (42 kDa), VIMENTIN (57 kDa), and GAPDH (36 kDa) in these cells. Immunoblots shown represent one of three independent

(legend continued on next page)

apparent in the liver sections of the CCl_4+sEV group whereas these cells were rarely detected in other groups (Figure 8D). Especially, HSC-like cells having process were positive, indicating that sEVs having miR-486-5p were successfully delivered into these cells (shown in the magnified image). The upregulation of *Smo* and *Gli2* in fibrotic livers significantly decreased in the sEV-treated livers with CCl_4 (Figure 8C). The protein levels of Smo and Gli2 confirmed the RNA data by showing significant reduction in the CCl_4+sEV group compared with other CCl_4-treated groups (Figure 8E). IHC for Gli2 also presented less accumulation of Gli2-positive cells in the CCl_4+sEV group compared with the CCl_4 and CCl_4+PBS group (Figure 8F). In addition, direct action of miR-486-5p was investigated in mice with acute liver damage caused by CCl_4. Liver injury was ameliorated in miR-486-5p-treated mice injected with CCl_4 (CCl_4+miR-486-5p group) compared with Scr-RNA-treated mice with liver injury (CCl_4+Scr group) (Figures S4A–S4C). *miR-486-5p* was significantly upregulated, and *Smo*, *Gli2*, and fibrotic markers *α-Sma*, *Vimentin*, *Ctgf*, and *Col1α1* were significantly downregulated in the liver tissues of the CCl_4+miR-486-5p group compared with the livers of the CCl_4+Scr group (Figure S4D). In line with RNA data of fibrotic markers, Sirius red staining and IHC for α-Sma clearly showed the decreased hepatic fibrosis and HSC activation in the CCl_4+miR-486-5p group compared with the CCl_4+Scr group (Figure S4E). These results support the inhibitory action of miR-486-5p targeting Smo in liver fibrosis.

To further verify the contribution of miR-486-5p to the reduced liver fibrosis mediated by T-MSC-sEVs, miR-486-5p in these sEVs was suppressed by miR-486-5p inhibitor. After confirming miR-486-5p knockdown in T-MSC-sEVs transfected with miR inhibitor, not in T-MSC-sEVs with Scr-miR (miR inhibitor negative control [NC]) (Figure S5A), these transfected sEVs were given to mice with acute liver injury by CCl_4 (Figure S5B). Because liver morphology, serum ALT/AST levels, and the expressions of Smo and fibrotic genes were similar among the CON, CON+PBS, and CON+sEV groups or between the CCl_4 and CCl_4+PBS groups (data not shown), the CON+sEV and CCl_4+PBS groups were used as the comparison groups in the analysis. sEVs with (CCl_4+sEV-NC group) or without NC (CCl_4+sEV group) attenuated liver injury caused by CCl_4, whereas T-MSC-sEVs transfected with miR-486-5p-inhibitor (CCl_4+sEV-miR-486-5p inhibitor group) rarely reduced liver damages in CCl4-injected mice (Figures S5C and S5D). Upregulated *miR-486-5p* and downregulated *Smo* in the CCl_4+sEV and CCl_4+sEV-NC groups were significantly alleviated and elevated, respectively, in the CCl_4+sEV-miR-486-5p inhibitor group (Figure S5E). Decreased expressions of fibrotic markers in the CCl_4+sEV and CCl_4+sEV-NC groups compared with the CCl_4+PBS group were also upregulated in the CCl_4+sEV-miR-486-5p inhibitor group (Figure S5F). Sirius red staining confirmed the fibrotic change in these groups by showing the apparent collagen accumulation in the livers of mice receiving CCl_4 with or without T-MSC-sEV transfected with miR-486-5p inhibitor (Figure S5G). These results demonstrate that miR-486-5p plays a critical role in mediating the effect of T-MSC-derived sEVs on liver fibrosis. Taken together, these results suggest that T-MSCs release sEVs harboring miR-486-5p, which inhibits the activation of HSCs by suppressing the Hh pathway, contributing to alleviating liver fibrosis.

DISCUSSION

The therapeutic effects of MSCs on human diseases, including liver disease, have been studied in numerous experimental and clinical studies.[4] Bone marrow has been the most widely used source of MSCs; however, the use of these cells in clinical applications has been limited due to the methodology of BM-MSC isolation, e.g., low cell yields, and donor pain caused by the invasive procedures for obtaining these cells.[33] To overcome this problem, it would be desirable to find alternative sources of MSCs, such as adipose tissue, umbilical cord blood, and the placenta. Recently, the human palatine tonsil has been identified as a new source of MSCs because tonsillectomy is the most common operative procedure in the field of otolaryngology, and T-MSCs can be easily obtained from surgically removed tonsil tissues.[12] In addition, T-MSCs share common characteristics with BM-MSCs and A-MSCs, such as similar morphology, the same surface markers, and the potential for proliferation and differentiation.[11,12] In particular, it has been reported that the proliferative ability of T-MSCs is much higher than that of BM-MSCs and A-MSCs, suggesting that T-MSCs are able to facilitate a large-scale production of MSCs.[13] Hence, it is highly possible that T-MSCs could be a stem cell source for treating liver disease. In the current study, we have shown that T-MSCs inhibit HSC activation and ameliorate chronic liver fibrosis in mice. Enriched miR-486-5p in sEVs released from T-MSCs targets Smo and suppresses Hh signaling, thus inactivating HSCs. Therefore, our results indicate that T-MSCs and T-MSC-derived sEVs can be a novel treatment against liver fibrosis.

HSC activation is the main event in liver fibrosis. Following liver injury, HSCs undergo an activation process and finally produce ECM.[1,2] Park et al.[17] demonstrated that infused T-MSCs migrate to the damaged liver where MSCs differentiate into hepatocyte-like cells and ameliorate liver fibrosis by promoting autophagy activation in parenchymal cells in mice with acute liver injury caused by CCl_4. They also reported that CM from T-MSCs relieves CCl_4-induced liver fibrosis in mice by attenuating liver inflammation.[18] However, no direct evidence of T-MSC action on HSC activation has been presented, and it remains unclear how infused T-MSCs affect HSC activation. In addition, their effect needs to be proven in a chronic model

experiments with similar results. Band densities were normalized to the expression level of GAPDH, which was used as an internal control. Data are presented as mean ± SEM from three identical experiments (unpaired two-sample Student's t test; *$p < 0.05$, **$p < 0.005$). (C) Representative images for PKH67-labeled sEVs (green) in human pHSCs, which were treated with vehicles (PBS) or T-MSC-sEVs (100 μg/mL) for 2 and 4 h. Hoechst 33342 was used for staining the nuclei of cells (original magnification, ×40; scale bars, 20 μm).

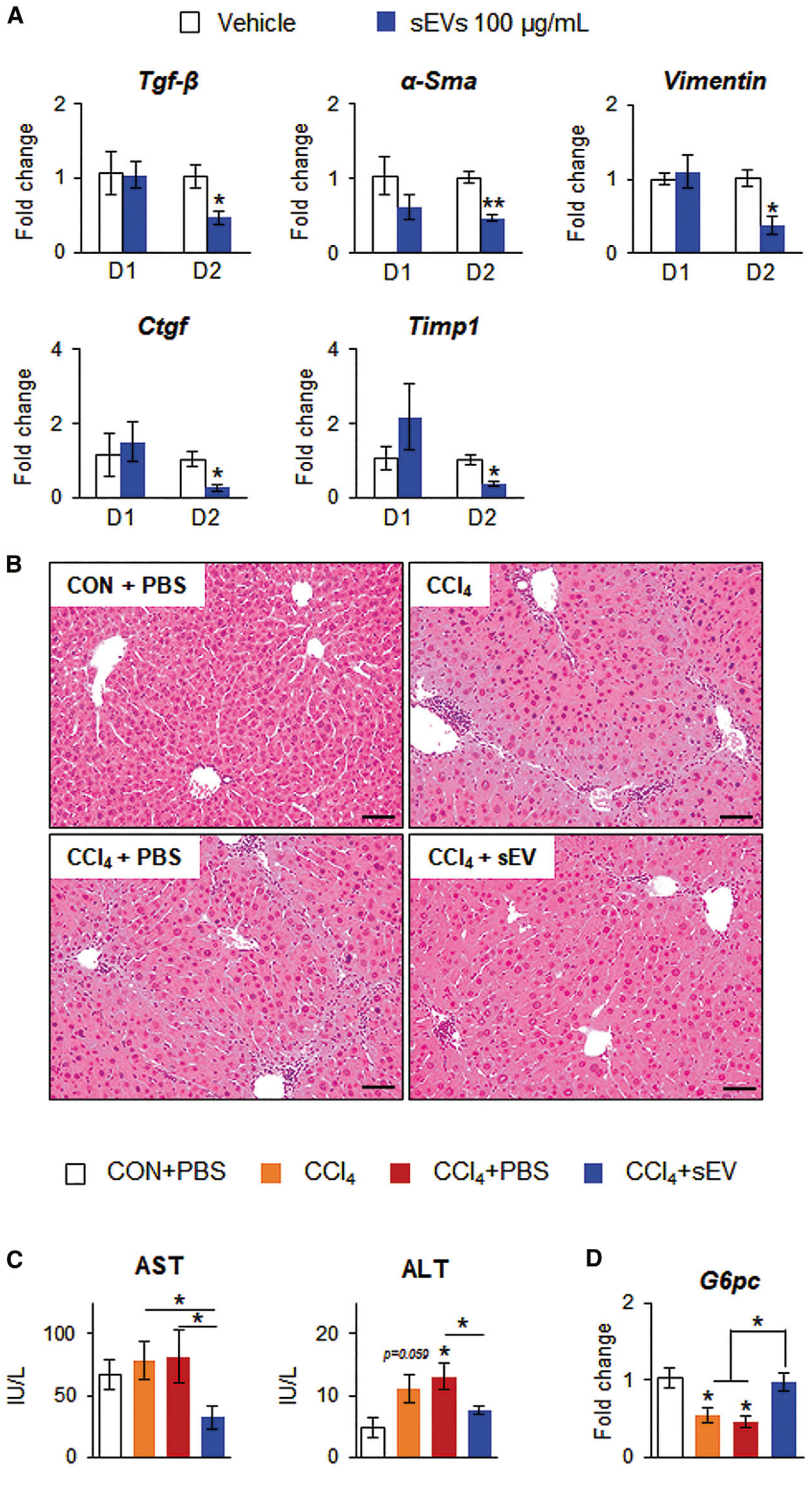

Figure 4. Administration of T-MSC-derived sEVs ameliorates CCl_4-induced liver injury in mice

(A) qRT-PCR analysis for *Tgf-β*, *α-Sma*, *Vimentin*, *Ctgf*, and *Timp1* in primary HSCs that were isolated from the livers of mice given CCl_4 and treated with vehicle (PBS) or T-MSC-derived sEVs (100 μg/mL) for 1 day (D1) or 2 days (D2). Data are presented as mean ± SEM of experiments performed in triplicate (unpaired two-sample Student's t test; *$p < 0.05$, **$p < 0.005$ versus own control). (B) Representative images of hematoxylin and eosin-stained liver sections from representative CON+PBS, CCl_4, CCl_4+PBS, and CCl_4+sEV groups (original magnification, ×10; scale bars, 100 μm). (C) The serum levels of AST and ALT from each group (CON+PBS, n = 3; CCl_4, n = 4; CCl_4+PBS, n = 4; and CCl_4+sEV, n = 5). Data are presented as mean ± SEM (unpaired two-sample Student's t test; *$p < 0.05$). (D) qRT-PCR of *G6pc* in the livers from each group (CON+PBS, n = 3; CCl_4, n = 4; CCl_4+PBS, n = 4; and CCl_4+sEV, n = 5). Data are presented as mean ± SEM (unpaired two-sample Student's t test; *$p < 0.05$).

to demonstrate T-MSCs as one of the MSC therapeutic sources. In the present study, we have demonstrated that T-MSCs directly inhibit HSC activation. Treatment with T-MSC-CM or coculture with T-MSCs reduced the levels of profibrotic genes in HSCs (Figure S1; Figure 1). Moreover, our results show that sEVs derived from T-MSCs directly inactivate HSCs, which are activated during culture and in fibrosis, as well as reduce liver fibrosis *in vivo* in chronically damaged livers (Figures 3, 4, and 5). These results clearly indicate that T-MSCs and their sEVs regulate HSC activation to suppress liver fibrosis and suggest the therapeutic potential of T-MSCs for treating liver fibrosis.

Growing evidence indicates that the therapeutic effects of MSC therapy are mediated by secretory factors that MSCs produce and release, and these secretory factors are called the MSC secretome.[34] Because sEVs are a part of the MSC secretome, it has been reported that sEVs released from MSCs are highly involved in the regenerative properties of MSCs.[22,23] In line with these findings, our results indicate that sEVs derived from T-MSCs, one of the sources of MSCs, also have antifibrotic and regenerative effects in chronic liver disease. Administration of sEVs derived from T-MSCs improved liver histomorphology and function as well as reduced collagen deposition in the livers of CCl_4-treated mice (Figures 4 and 5). In addition, our results showed that sEVs have no undesirable toxicity in a liver that is not injured (Figure S2). These results support the notion that sEVs could be a promising cell-free therapeutic strategy in the treatment of liver disease. Currently, there has been growing interest in research on sEVs because of their potential in regenerative medicine.[22,35] However, progress has been held back by challenges such as difficulties in isolation and characterization of sEVs, despite significant efforts made in this novel field of research.[36] In the current study, we isolated sEVs by

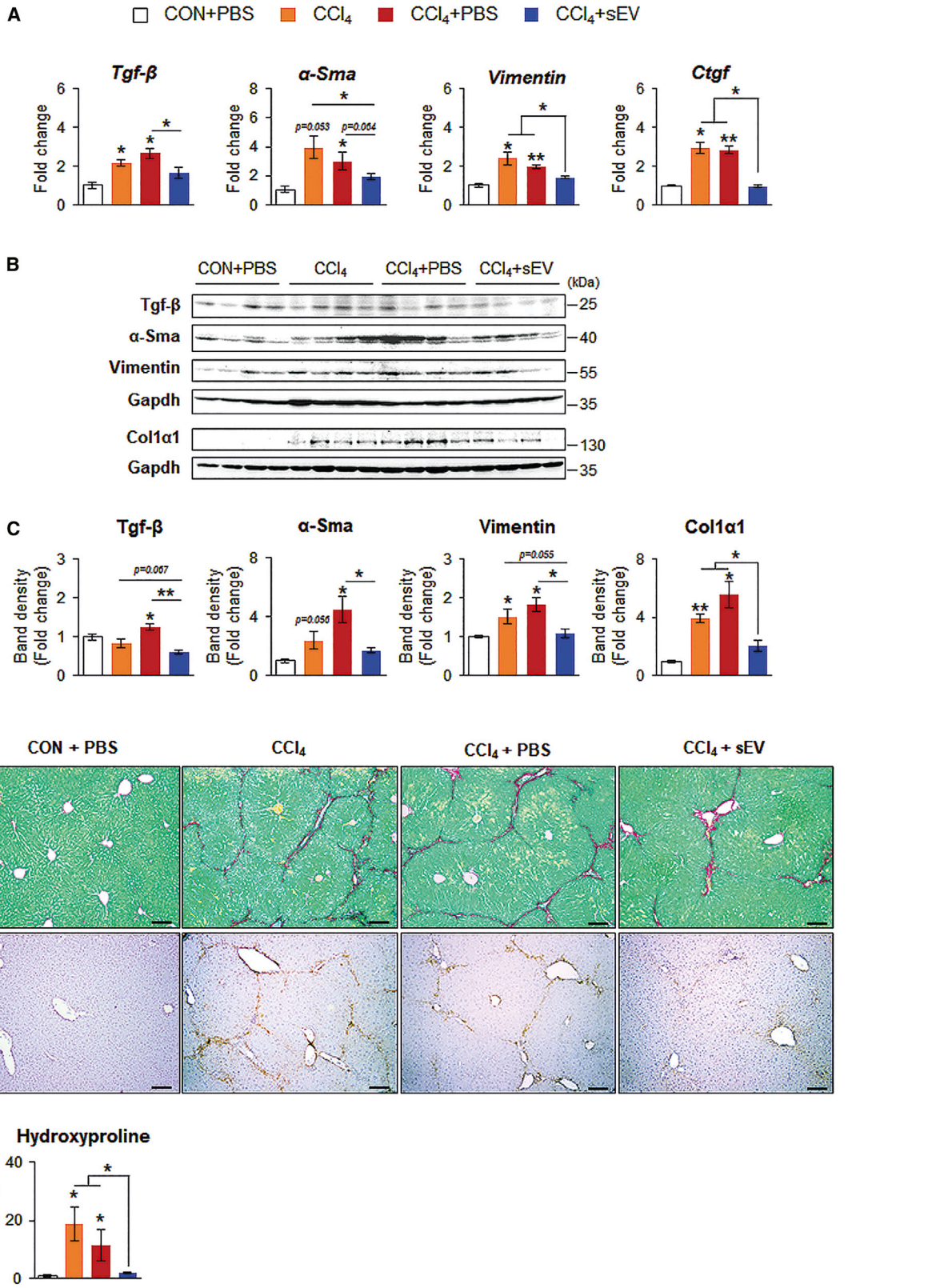

(legend on next page)

ultracentrifugation, which is the most established and widely used method,[37] and characterized them by their size, shape, and surface markers (Figure 2) to verify the quality of the isolated sEVs. DLS analysis showed that the size range of isolated sEVs was from 50 to 290 nm. Since DLS can also recognize aggregated sEVs as a single sEV,[38,39] the actual size of sEVs may be different from the size measured by DLS. Hence, the sEVs were additionally checked by TEM analysis, and a single sEV with a cup-shaped morphology showed a diameter range between 50 and 100 nm. The presence of sEV surface markers such as CD63, CD81, and CD9 and the absence of calreticulin also confirmed the identity of the sEVs isolated in our system. These results clearly support the homogeneity and reliability of the isolated sEVs used in this study.

miRNAs are small noncoding RNAs that regulate gene expression by binding to target mRNAs and interfering with their translation.[40] sEVs play a major role in cell-to-cell communication by transferring bioactive molecules, including miRNAs.[21] Since miRNAs are selectively packaged into sEVs and secreted extracellularly, the presence and composition of miRNAs in sEVs indicate that they serve as intracellular messengers in a cell-specific manner.[19,21] Microarray data from a previous study showed that miR-486-5p is an abundant miRNA in human MSCs, including A-MSCs, BM-MSCs, and T-MSCs.[13,29] In addition, Baglio et al.[41] reported that miR-486-5p is abundant in exosomes derived from BM-MSCs and A-MSCs. However, it remains unknown whether miR-486-5p is contained in sEVs derived from T-MSCs. Herein, we found that miR-486-5p is highly enriched in sEVs derived from MSCs compared with other candidate miRNAs (Figure 6), and the level of miR-486-5p in T-MSC-derived sEVs was markedly higher than that in normal liver and activated HSCs. Interestingly, the amount of miR-486-5p in sEVs from T-MSCs was approximately 300-fold higher than that in T-MSCs. These results indicate that miR-486-5p produced by T-MSCs is preferentially packaged into their sEVs and secreted extracellularly. Our results support this hypothesis by showing that after treatment with sEVs, the level of miR-486-5p is significantly elevated in both pHSCs and damaged liver (Figure 8). Transferred miR-486-5p into pHSCs directly targets Smo and inactivates Hh signaling in these cells. Given that Hh signaling is a major regulator of HSC activation, miR-486-5p enrichment in sEVs released from T-MSCs modulates HSC activation by regulating Hh signaling, indicating how T-MSCs affect HSCs and the liver. However, the mechanism underlying the selective packing of miRNAs into sEVs is largely unknown, and further studies are needed.

In conclusion, we demonstrated that T-MSCs and their sEVs suppress HSC activation and liver fibrosis. sEVs derived from T-MSCs contain miR-486-5p, which inactivates HSCs by suppressing Hh signaling. Therefore, our findings suggest that T-MSCs could be a novel source for MSC therapy and that T-MSC-derived sEVs have great potential as an effective antifibrotic therapeutic agent for treating chronic liver disease.

MATERIALS AND METHODS

Cell experiments

Human primary T-MSCs (provided by Dr. B.J. Lee, Pusan National University Hospital, Korea) were cultured in minimum essential medium alpha (MEMα; Gibco, Thermo Fisher Scientific, MA, USA) supplemented with 10% fetal bovine serum (FBS; Gibco) and 1% penicillin/streptomycin (P/S; Gibco) at 37°C in a humidified atmosphere containing 5% CO_2. LX2, a human HSC line (provided by Dr. W.-I. Jeong, Korea Advanced Institute of Science and Technology, Korea), human pHSCs (purchased from Zen-Bio, NC, USA), and HepG2, a human hepatocellular carcinoma cell line (provided by Dr. S.-W. Kim, Pusan National University, Korea), were cultured in Dulbecco's Modified Eagle Medium (DMEM; Gibco) supplemented with 10% FBS (Gibco) and 1% P/S (Gibco) at 37°C in a humidified atmosphere containing 5% CO_2. For preparation of CM, T-MSCs were seeded on 10-cm^2 plates at 70% confluence. The next day, cells were washed with PBS twice, changed with 0.1% FBS-containing medium, and incubated for 72 h. Then, CM was collected for subsequent experiments. To evaluate the effects of T-MSC-CM on LX2, LX2 cells at 70% confluence were serum starved in medium containing no FBS overnight and cultured in T-MSC-CM for 24 or 48 h. Co-cultures between pHSCs and T-MSCs were conducted using Transwell inserts (Corning, NY, USA) in which culture medium was diffusible but cells were not permeable. All co-culture experiments were performed with pHSCs seeded in the bottom wells, and T-MSCs seeded in the top wells. Insert chambers with T-MSCs were transferred into a co-culture system and cultured for 24 or 48 h. To examine the effect of miR-486-5p on HSC activation, pHSCs at 70% confluence were serum starved in medium containing no FBS overnight and cultured in medium containing 2% FBS and no P/S for 24 h. Then, cells were transfected with 25 nM miR-486-5p mimic (Bioneer, Daejeon, Korea) or Scr-miR (Bioneer) as an NC using Lipofectamine RNAiMAX transfection reagent (Invitrogen, Thermo Fisher Scientific) according to the manufacturer's instructions. After 6 h, the medium was changed with fresh medium containing 2% FBS and 1% P/S, and then these transfected cells were incubated for 24 or 48 h.

Figure 5. Hepatic fibrosis is alleviated in mice given CCl_4 with T-MSC-derived sEVs

(A) qRT-PCR analysis of *Tgf-β*, *α-Sma*, *Vimentin*, and *Ctgf* in the livers from CON+PBS, CCl_4, CCl_4+PBS, and CCl_4+sEV groups (n = 3 per group). Data are presented as mean ± SEM (unpaired two-sample Student's t test; *p < 0.05, **p < 0.005). (B and C) Western blot (B) and cumulative densitometric (C) analyses of Tgf-β (25 kDa), α-Sma (42 kDa), Vimentin (57 kDa), Col1α1 (140 kDa), and Gapdh (36 kDa) in the livers from each group (n = 4 per group). Immunoblots shown represent one of three independent experiments with similar results. Band densities were normalized to the expression level of GAPDH, which was used as an internal control. Data are presented as mean ± SEM (unpaired two-sample Student's t test; *p < 0.05, **p < 0.005). (D) Representative images of Sirius-red-stained (top) and α-Sma-stained (bottom) liver sections from each group (original magnification, ×10; scale bars, 100 μm). (E) Relative levels of hydroxyproline contents in the livers from each group (CON+PBS, n = 4; CCl_4, n = 4; CCl_4+PBS, n = 5; and CCl_4+sEV, n = 6). Data are presented as mean ± SEM (unpaired two-sample Student's t test; *p < 0.05).

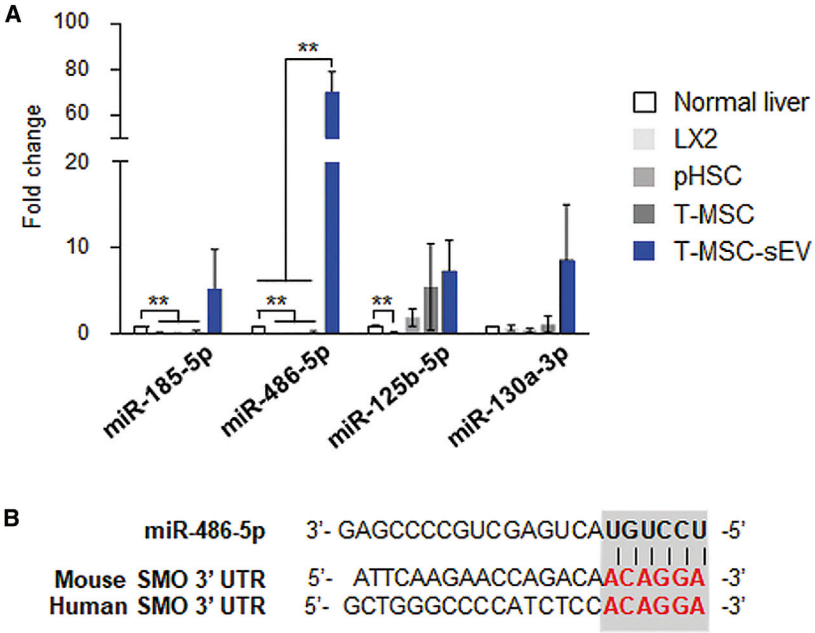

Figure 6. miR-486-5p is highly enriched in T-MSC-derived sEVs and directly targets to SMO

(A) qRT-PCR analysis of *miR-185-5p*, *miR-486-5p*, *miR-125b-5p*, and *miR-130a-3p* in human normal liver tissues, LX2, pHSCs, T-MSCs, and T-MSC-derived sEVs. Data are presented as mean ± SEM (unpaired-two sample Student's t test; **p < 0.005). (B) Using a miRNA database (miRWalk), the potential binding site (red fonts) of miR-486-5p was predicted in the 3′ UTR of *SMO* mRNA in mice and humans. The dashed line represents complementary base pairs between miR-486-5p and SMO mRNA, whereas the gray shading indicates the seed sequence of miR-486-5p. (C) A dual-luciferase assay was performed to verify binding interaction between miR-486-5p and SMO mRNA. HepG2 or LX2 was co-transfected with psi-CHECK-2 vector containing either wild-type (WT) or mutant (mut) target sites plus either the miR-486-5p mimic or scrambled (Scr-)miR (control). Results of relative luciferase assay activity are shown as mean ± SEM obtained from triplicate experiments (unpaired two-sample Student's t test; *p < 0.05 versus own control).

sEV isolation and characterization

sEVs were isolated by differential centrifugation as previously described.[37] Briefly, T-MSCs were seeded onto 10-cm^2 plates at a density of 6 × 10^5 cells and allowed to grow to 70% confluence. Then, cells were washed with PBS twice and cultured in MEMα containing 10% FBS devoid of sEVs for 48 h. For elimination of sEVs from FBS, FBS was centrifuged at 110,000 × *g* overnight at 4°C. Then, cultured media were collected and centrifuged at 300 × *g* for 10 min, followed by centrifugation at 2,000 × *g* for 20 min to remove cells and cellular debris. The culture media obtained from a total of 18 culture dishes was used when sEVs were isolated. Then, cell-free supernatants were transferred to ultra-clear tubes and centrifuged at 10,000 × *g* for 30 min using an ultracentrifuge (Optima L-90K; Beckman Coulter, CA, USA) equipped with a type 90 Ti fixed-angle rotor (355530; Beckman Coulter). Next, the supernatants were centrifuged at 110,000 × *g* for 90 min to precipitate pellets containing sEVs. sEV-containing pellets were washed with PBS and centrifuged at 110,000 × *g* for 90 min. Finally, the resulting pellet was carefully resuspended in PBS and its concentration was measured. The concentration of sEVs was maintained at the constant level in each round of sEV preparation (average 800 μg per each sEV preparation). The sEVs resuspended in PBS were used immediately or stored at −80°C. All steps were conducted at 4°C. To characterize the sEVs, the diameter of isolated sEVs was measured by DLS using a Zetasizer Nano S (Malvern Instruments, Malvern, UK) or visualized by TEM (Tecnai F20 G2, FEI, Hillsboro, OR, USA). For detecting sEV surface markers, isolated sEVs were analyzed by western blotting with antibodies specific to CD63 (Santa Cruz Biotechnology, TX, USA), CD9 (Abcam, Cambridge, UK), CD81 (Santa Cruz Biotechnology), and calreticulin (Abcam).

In vitro treatment of T-MSC-derived sEVs

After serum starvation for 6 h in FBS-free medium, human pHSCs at 70% confluence were treated with isolated sEVs at different concentrations (0, 1, 10, and 100 μg/mL) or vehicle (PBS) for 24 and 48 h. The concentration of sEVs was assessed using a Pierce bicinchoninic acid (BCA) protein assay kit (Thermo Fisher Scientific). To investigate the effects of T-MSC-derived sEVs on *in vivo*-activated HSCs, primary activated HSCs were isolated from fibrotic liver of mice injected with CCl_4 (0.4 mL/kg body weight) three times a week for 5 weeks by *in situ* perfusion with EGTA and by collagenase and

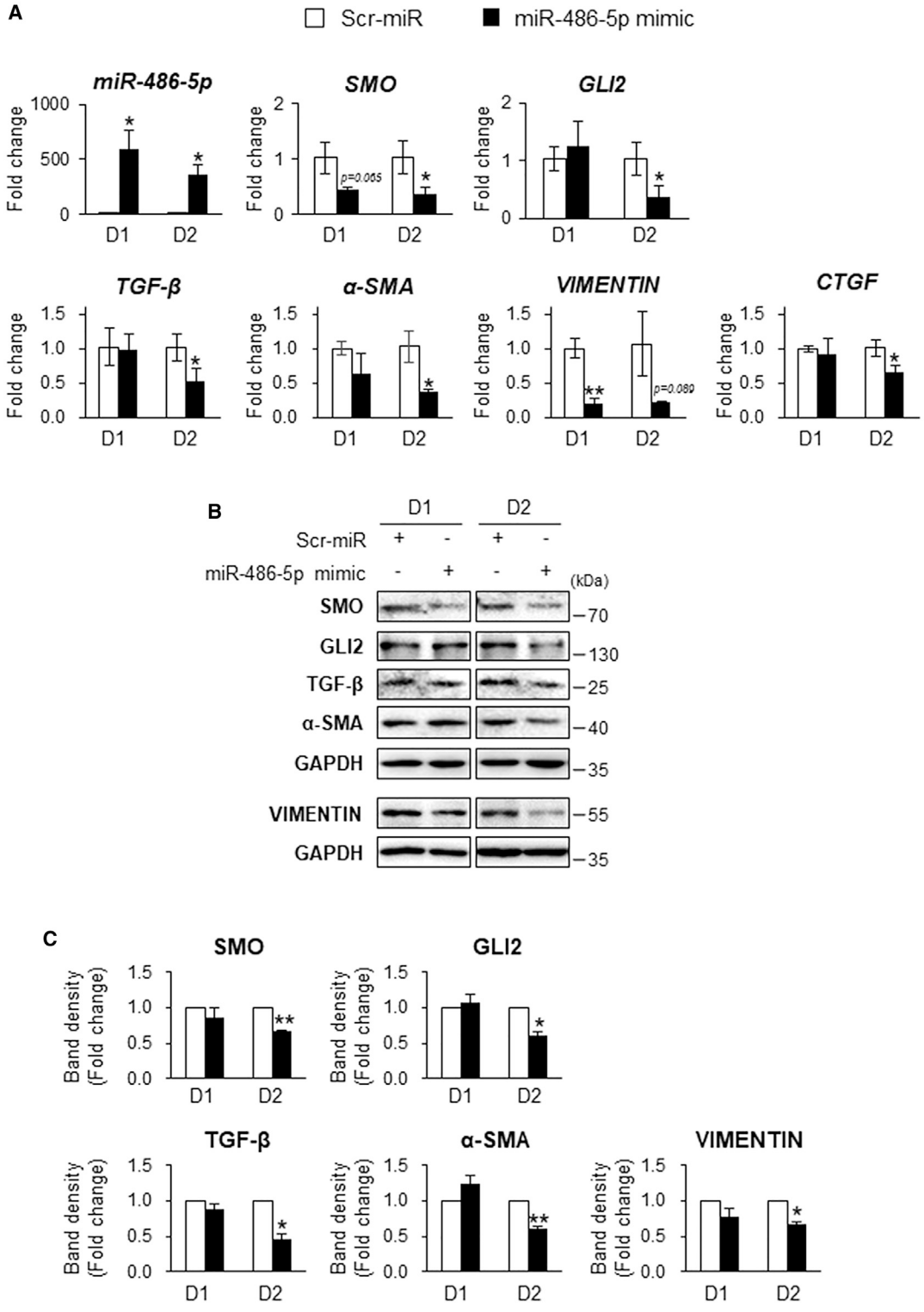

Figure 7. miR-486-5p decreases expression of HSC activation markers and Hh-activated genes

(A) qRT-PCR analysis of *miR-486-5p*, *SMO*, *GLI2*, *α-SMA*, *VIMENTIN*, *CTGF*, and *TGF-β* in pHSCs transfected with Scr-miR or miR-486-5p mimic for 1 day (D1) or 2 days (D2). All data are presented as mean ± SEM obtained from triplicate experiments (unpaired two-sample Student's t test; *p < 0.05). (B and C) Western blot (B) and cumulative

(legend continued on next page)

subsequent OptiPrep density gradient centrifugation as previously described. Activated murine pHSCs were starved for 6 h in FBS-free medium and then treated with T-MSC-derived sEVs at a concentration of 100 μg/mL or vehicle for 24 and 48 h.

Uptake studies of sEVs by pHSCs

sEVs isolated from T-MSCs were labeled with green fluorescence using a PKH67 green fluorescent cell linker kit (Sigma-Aldrich, MO, USA) according to the manufacturer's instruction. In brief, isolated sEVs were incubated with PKH67 fluorescent dye for 5 min at room temperature (RT). Then, unconjugated fluorescent dye was washed out by ultracentrifugation at 110,000 × *g* for 2 h at 4°C. Thereafter, the resulting pellet resuspended in PBS was used immediately. Human pHSCs were seeded on coverslips in six-well culture plates at a density of 1×10^4 cells. After serum starvation for 6 h in FBS-free medium, cells were treated with fluorescently labeled sEVs (100 μg/mL) or vehicle (PBS) for 2 and 4 h. Then, the nuclei of the cells were stained with Hoechst 33342 (Thermo Fisher Scientific) for confocal microscopy imaging. The uptake of sEVs was imaged by using a confocal microscope (Carl Zeiss, Thornwood, NY, USA).

Transfection of miR-486-5p inhibitor into sEVs

sEVs isolated from T-MSCs were transfected with human miR-486-5p inhibitor (5′-UCC UGU ACU GAG CUG CCC CGA G-3′; Bioneer) or miR inhibitor NC (Bioneer) using an Exo-Fect exosome transfection reagent kit (EXFT20A-1, System Biosciences, Palo Alto, CA, USA) according to the manufacturer's instructions. Briefly, 300 μg of sEVs was incubated with a mixture of the Exo-Fect transfection reagent and miR-486-5p inhibitor (20 pmol) or NC inhibitor at 37°C for 10 min. Next, supernatant was removed by centrifugation at 14,000 rpm for 3 min, and the resulting pellets containing transfected sEVs were resuspended in PBS for further experiments.

Experimental animal models

Male C57BL/6 mice were purchased from Hyochang (Dae-gu, Korea), housed with a 12-h light/12-h dark cycle and allowed free access to normal food and water. To examine the effect of T-MSC-derived sEVs on liver fibrosis, 6-week-old mice received 0.4 mL/kg body weight of CCl_4 (Jin Chemical Pharmaceutical, Seoul, Korea) dissolved in corn oil by intraperitoneal injection, three times a week for 2 weeks (n = 15). As a control, mice were injected with equal volume of corn oil (CON) (n = 13). Next, mice in the CCl_4 group were randomly divided into three experimental groups, which were treated with 0.4 mL/kg body weight of CCl_4 twice a week for 3 weeks only (CCl_4 group; n = 4), and in parallel with intravenous injection of PBS (CCl_4+PBS group; n = 5) or T-MSC-derived sEVs once a week (150 μg per mouse, CCl_4+sEV group; n = 6). In the same way, corn oil-injected mice were randomly divided into three experimental groups, that is, the CON group (n = 4), the CON+PBS group (n = 4), and the CON+sEV group (n = 5). To obtain serum and liver tissues, all mice were sacrificed after 48 h of the last injection of T-MSC sEVs. To examine the direct effect of miR-486-5p in mice with acute liver injury, 7-week-old male C57BL/6 mice received 1.0 mg/kg body weight of CCl_4 (n = 10) intraperitoneally twice for 1 week and then injected intraperitoneally with 8 nmol per mice of miR-486-5p mimic (n = 5) or Scr-miR (n = 5) using *in vivo*-jetPEI (Polyplus Transfection, Illkirch, France) at day 8. As controls, corn oil-injected mice (n = 8) were also treated with miR-486-5p mimic (n = 4) or Scr-miR (n = 4). To assess the contribution of sEV-miR-486-5p to the anti-fibrotic effect of T-MSCs in mice with acute liver injury, 7-week-old male C57BL/6 mice received 1.0 mg/kg body weight of CCl_4 (n = 28) intraperitoneally twice for 1 week (Figure S5B). Next, mice in CCl_4 groups were randomly divided into five experimental groups. As CCl_4 CON groups, mice were treated with (CCl_4+PBS, n = 5) or without PBS (CCl_4, n = 5), and as sEV-receiving CON groups, mice were injected intravenously with 150 μg of T-MSC-sEVs (CCl_4+sEV, n = 6) or T-MSC-sEVs transfected with either NC (CCl_4+sEV-NC, n = 6) or miR-486-5p inhibitor (CCl_4+sEV-miR-486-5p inhibitor, n = 6) per mouse at day 8. As corn oil-receiving controls, corn oil-injected mice were also treated with vehicle (n = 4), T-MSC-sEVs (n = 4), or nothing (n = 3). All mice in the acute injury model were sacrificed at day 11. At the time of sacrifice, mice were weighed, and blood samples were collected under isoflurane inhalation by sterile cardiac puncture. Mice were then euthanized humanely under anesthesia by cervical dislocation, and livers were promptly dissected from the animal. All animal care and surgical procedures were approved by the Pusan National University Institutional Animal Care and Use Committee and were carried out according to the provisions of the National Institutes of Health (NIH) *Guidelines for the Care and Use of Laboratory Animals*.

RNA analysis

Total RNAs were extracted from cells, liver tissues, or sEVs by using TRIzol reagent (Ambion, Thermo Fisher Scientific). The purity and concentration of RNA were determined using a NanoDrop spectrophotometer. Template cDNA was synthesized from total RNA using a SuperScript II first-strand synthesis system (Invitrogen) or HB_I RT reaction kit (HeimBioteck, Seongnam, Korea) according to the manufacturers' instructions. qRT-PCR was performed by using Power SYBR Green master mix (Applied Biosystems, Thermo Fisher Scientific) or HB_I real-time PCR master mix (HeimBioteck) according to the manufacturer's specifications (Mastercycler realplex real-time PCR, Eppendorf, Hamburg, Germany). All reactions were performed in triplicate, and data were analyzed according to the $\Delta\Delta C_t$ method. For normalization of expression level, 40S ribosomal protein S9

densitometric (C) analyses of SMO (86 kDa), GLI2 (133 kDa), TGF-β (25 kDa), α-SMA (42 kDa), VIMENTIN (57 kDa), and GAPDH (36 kDa) in these cells. GAPDH was used as an internal control. Immunoblots shown represent one of three independent experiments with similar results. Band densities were normalized to the expression level of GAPDH, which was used as an internal control. Data are presented as mean ± SEM from three identical experiments (unpaired two-sample Student's t test; *$p < 0.05$, **$p < 0.005$ versus own control).

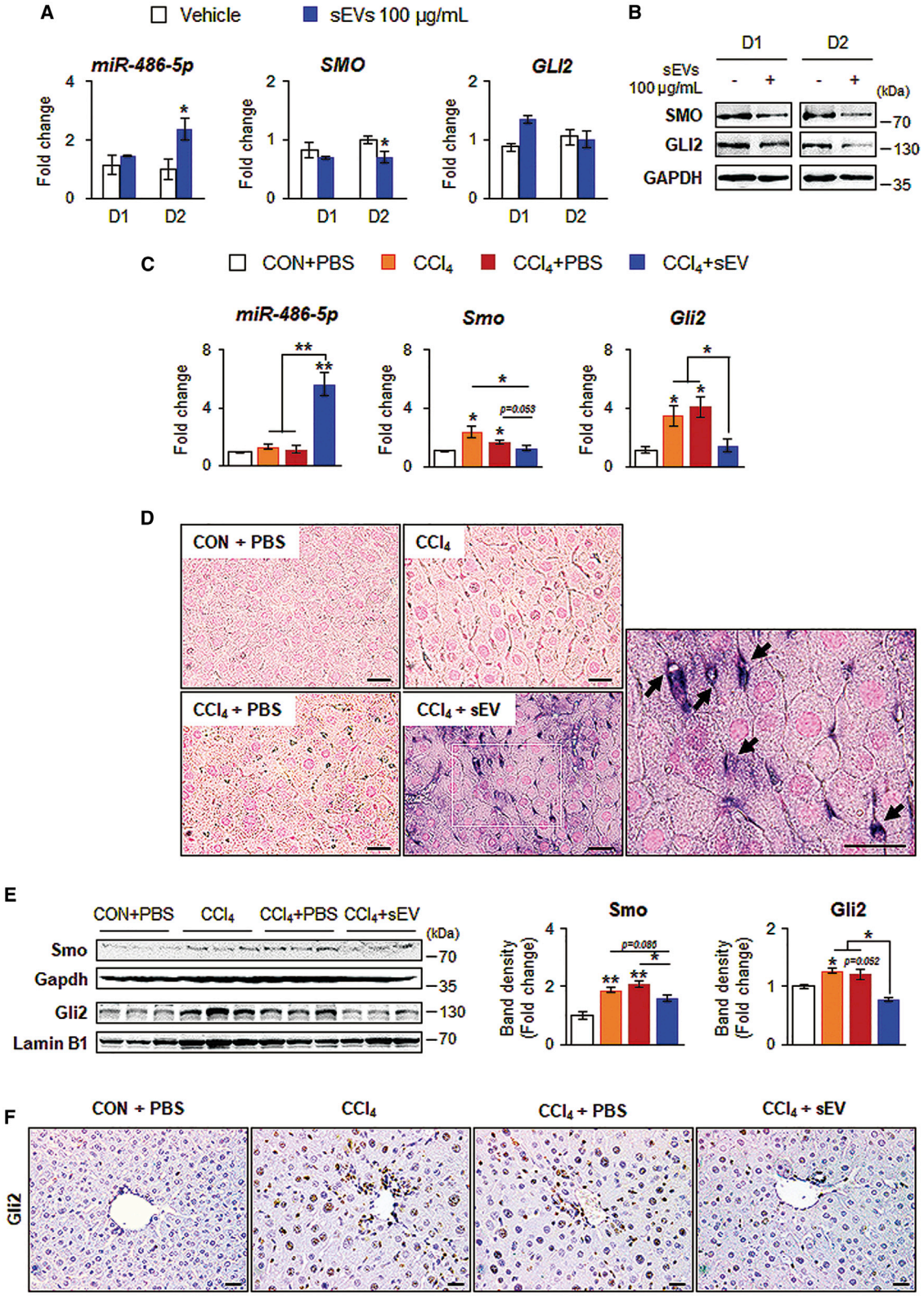

(legend on next page)

mRNA and U6B small nuclear RNA (RNU6B) were used for mRNA and miRNA, respectively. The sequences of all primers used in evaluating mRNA expression are listed in Table S1. Commercially predesigned primers for miR-185-5p, miR-125b-5p, miR-486-5p, and miR-130a-3p were purchased from HeimBioteck. All PCR products were directly sequenced for genetic confirmation (Macrogen, Seoul, Korea).

Western blot analysis

Total protein was extracted from cells, liver tissues, or sEVs in Triton lysis buffer (TLB) supplemented with protease inhibitors (Complete Mini 11 836 153 001; Roche, Indianapolis, IN, USA). For Gli2 detection in liver tissues, nuclear fractionation was performed as described previously.[42] The concentration of protein was measured by a Pierce BCA protein assay kit (Thermo Fisher Scientific). Equal amounts of total protein were separated by 8% or 10% SDS-PAGE and transferred onto a polyvinylidene fluoride (PVDF) membranes (Millipore, Darmstadt, Germany). Primary antibodies used in this study were as follows: CD63 (diluted 1:200; sc-5275, Santa Cruz Biotechnology), CD9 (diluted 1:500; ab92726, Abcam), CD81 (diluted 1:200; sc-16602, Santa Cruz Biotechnology), calreticulin (diluted 1:1,000; ab2907, Abcam), TGF-β (diluted 1:1,000; 3711S, Cell Signaling Technology, MA, USA), α-SMA (diluted 1:1,000; A5228, Sigma-Aldrich), VIMENTIN (diluted 1:1,000; sc-5565, Santa Cruz Biotech.), COL1α1 (diluted 1:1,000; NBP1-30054, Novus Biologicals, CO, USA), GFAP (diluted 1:1,000; Z0334, Dako, Carpinteria, CA, USA), SMO (diluted 1:1,000; ab72130, Abcam), GLI2 (diluted 1:1,000; GWB-CE7858, GenWay Biotech, CA, USA), LAMIN B1 (diluted 1:1,000; ab16048, Abcam), and GAPDH (diluted 1:1,000; MCA4739, AbD Serotec, Oxford, UK). Horseradish peroxidase (HRP)-conjugated anti-rabbit (ADI-SAB-300-J, Enzo Life Sciences, NY, USA) and anti-mouse immunoglobulin G (IgG) (ADI-SAB-100-J, Enzo Life Sciences) were used as secondary antibodies. Protein bands were detected using an EzWestLumi enhanced chemiluminescence (ECL) solution (ATTO, Tokyo, Japan) as per the manufacturer's specifications (EzCapture II, ATTO). The cumulative densitometric analysis of immunoblots was measured by CS Analyzer 4 software (ATTO).

Liver histology and IHC

Liver specimens were fixed in 10% neutral buffered formalin (Sigma-Aldrich), embedded in paraffin, and cut into 4-μm-thick sections. Sections were dewaxed, hydrated, and stained per standard protocols with standard H&E staining to examine morphology and Sirius red staining for fibrotic processes. For H&E staining, sections were stained in hematoxylin (Gill's hematoxylin V, Muto Pure Chemicals, Tokyo, Japan) for 15 min and then stained in eosin (1% eosin Y solution, Muto Pure Chemicals) for 5 min. For Sirius red staining, sections were incubated for 30 min in 0.1% Sirius red F3B (Sigma-Aldrich) containing saturated picric acid (Sigma-Aldrich) and 0.1% fast green (Sigma-Aldrich). For IHC, sections were incubated for 10 min in 3% hydrogen peroxide to block endogenous peroxidases. Antigen retrieval was performed by heating in 10 mM sodium citrate buffer (pH 6.0). After washing with Tris-buffered saline (TBS), sections were treated with Dako protein block (Dako) for 30 min and incubated with primary antibodies, anti-α-SMA antibody (ab5694; Abcam), and anti-GLI2 (GWB-CE7858; GenWay Biotech) at 4°C overnight. Additional sections were also incubated at 4°C overnight in non-immune sera to demonstrate staining specificity. HRP-conjugated anti-rabbit (K4003; Dako) secondary antibody was used. 3,3′-Diaminobenzidine (Dako) was used for the detection procedure. Slides were viewed with an Olympus CX41 light microscope (Olympus Optical, Tokyo, Japan), and morphometric analysis of stained regions in the tissue sections was performed using cellSens software (Olympus Optical).

In situ PCR

In situ PCR for miR-486-5p was performed as described previously.[43] Thin sections (4 μm) of paraffin-embedded liver tissue were dewaxed, hydrated, incubated in 0.2 M HCl for 10 min, and treated with 10 μg/mL proteinase K at RT for 20 min. Then, sections were subjected to heat-induced antigen retrieval in 10 mM sodium citrate buffer (pH 6.0). After washing slides with PBS, they were treated with 4% paraformaldehyde in PBS for 5 min and air-dried completely. Slides contained PCR mixtures (25 mM $MgCl_2$, 2.5 mM 2′-deoxynucleoside 5′-triphosphate [dNTP], 1 nM digoxigenin-11-deoxyuridine triphosphate [DIG-11-dUTP, Roche], anti-human miR-486-5p primer, and Taq polymerase in 1× PCR buffer) were sealed with coverslips and run for 40 cycles of PCR. After being washed with saline sodium citrate (SSC) and PBS, slides were fixed again in 4% paraformaldehyde in PBS for 5 min. After being washed with PBS and equilibrated in buffer 1 (100 mM Tris/150 mM NaCl [pH 7.5]), slides were incubated with alkaline phosphatase (AP)-coupled anti-DIG antibody (anti-DIG-AP Fab fragments; diluted 1:5,000; 11093274910; Roche) in Tris 100 mM/NaCl 150 mM (pH 7.5) buffer with 0.5%

Figure 8. miR-486-5p transferred by T-MSC-derived sEVs downregulates Hh-activated genes in pHSCs and damaged livers

(A) qRT-PCR analysis of *miR-486-5p*, *SMO*, and *GLI2* in human pHSCs treated with vehicles (PBS) or T-MSC-derived sEVs (100 μg/mL) for 1 day (D1) or 2 days (D2). Data are presented as mean ± SEM of experiments performed in triplicate (unpaired two-sample Student's t test; *$p < 0.05$ versus own control). (B) Western blot analysis of SMO (86 kDa) and GLI2 (133 kDa) in these cells. GAPDH (36 kDa) was used as an internal control. Immunoblots shown represent one of three independent experiments with similar results. (C) qRT-PCR analysis of *miR-486-5p*, *Smo*, and *Gli2* in livers from CON+PBS, CCl_4, CCl_4+PBS, and CCl_4+sEV groups (n = 3 per group). Data are presented as mean ± SEM (unpaired two-sample Student's t test; *$p < 0.05$, **$p < 0.005$). (D) *In situ* PCR for the human *miR-486-5p* gene in the livers of representative mice from these groups (original magnification, ×60, magnified images, ×120; scale bars, 20 μm). In the magnified images, black arrows indicate *miR-486-5p*-positive HSC-like cells colored blue/violet. (E) Western blot and cumulative densitometric analyses of Smo (86 kDa) and Gli2 (133 kDa) in the livers from each group. Immunoblots shown represent one of three independent experiments with similar results Band densities were normalized to the expression level of LAMIN B1 (66 kDa) or GAPDH (36 kDa), which was used as an internal control. Data are presented as mean ± SEM (unpaired two-sample Student's t test; *$p < 0.05$, **$p < 0.005$). (F) Representative images of Gli2-immunostained liver sections from representative mice from each group (original magnification, ×40; scale bars, 20 μm).

Boehringer Mannheim blocking reagent. After washing with buffer 1 and equilibration with buffer 3, AP-coupled DIG signals (blue/violet colors) in liver sections were developed with nitroblue tetrazolium/5-bromo-4-chloro-3-indolyl phosphate (NBT/BCIP) solution (Roche) in 100 mM Tris, 100 mM NaCl, and 50 mM $MgCl_2$ (pH 9.5) buffer at RT. Sections were counterstained with nuclear fast red (Vector Laboratories, Burlingame, CA, USA) and mounted in Cytoseal (Richard-Allan Scientific, Kalamazoo, MI, USA). Slides were viewed with an Olympus CX41 light microscope (Olympus Optical).

Measurement of AST/ALT

Serum AST/GOT (glutamate-oxaloacetate transaminase) and ALT/GPT (glutamate pyruvate transaminase) were measured using GOT and GPT reagents (Asan Pharmaceutical, Seoul, Korea) according to the manufacturer's instructions.

Hydroxyproline assay

Hydroxyproline contents of the livers were calculated by the method previously described.[42] Briefly, 50 mg of liver tissue was hydrolyzed in 6 N HCl at 110°C for 16 h. The hydrolysate was evaporated under vacuum and the sediment was re-dissolved in 1 mL of distilled water. Samples were filtered using a 0.22-μm filter tube at 14,000 rpm for 5 min. Lysates were then incubated with 0.5 mL of chloramine-T solution containing 1.41 g of chloramine-T dissolved in 80 mL of acetate-citrate buffer and 20 mL of 50% isopropanol at RT. After 20 min, 0.5 mL of Ehrlich's solution containing 7.5 g of dimethylaminobenzaldehyde dissolved in 13 mL of 60% perchloric acid and 30 mL of isopropanol was added to the mixture and incubated at 65°C for 15 min. After cooling at RT, the absorbance was read at 561 nm. The amount of hydroxyproline in each sample was determined using the regression curve from high-purity hydroxyproline (Sigma-Aldrich) and divided by the amount of liver weight to get the hydroxyproline contents (μg of hydroxyproline per mg of liver). Data were expressed as fold changes by comparing with the hydroxyproline content of the CON group.

Cloning of vector constructs and luciferase reporter assay

For cloning of vector constructs, target genes of human miR-486-5p were predicted by bioinformatics analysis using the online database http://mirwalk.umm.uni-heidelberg.de. The 3′ UTR of human *SMO* from genomic DNA, containing binding sites for human miR-486-5p, was amplified by PCR. The primers sequences used for vector construction were as follows: forward, 5′-TTT TCT CGA GGG GGC CAT GTC CTC TCT TAA-3′, reverse, 5′-TGC GGC CGC TTG GAG GCT ATG GAA GGT GG-3′. The PCR product was purified using an AccuPrep PCR purification kit (Bioneer), cut by the restriction enzymes Xho1 and Not1, and then cloned into the psiCHECK-2 vector (Promega, WI, USA). The vector constructs with 3′ UTR of *SMO* were transformed into *Escherichia coli*, and then plasmid DNA was extracted from well-transformed, ampicillin-resistant *E. coli*, using an AccuPrep plasmid mini extraction kit (Bioneer). The sequences of the miR-486-5p-binding sites of the 3′ UTR of *SMO* were confirmed by sequencing analysis (Macrogen). Mutant vectors lacking the miR-486-5p-binding site were manufactured by Enzynomics (Daejeon, Korea). For the luciferase reporter assay, HepG2 or LX2 cells were seeded in 24-well culture plates in culture medium without P/S 1 day before transfection. Using Lipofectamine 2000 (Invitrogen), cells were transfected with a mixture of psiCHECK-2 vector construct and either 25 nM miR-486-5p mimic (5′-UCC GUA UGA CUG CCC AG-3′; Bioneer) or scrambled miRNA (SMC-2003; Bioneer) as an NC. At 48 h after transfection, cells were harvested and tested with the Dual-Luciferase reporter assay system (Promega) according to the manufacturer's protocol. All firefly luciferase activity data are normalized to *Renilla* luciferase activity and presented as the mean ± SEM of values from at least three repetitive experiments.

Statistical analysis

Results are expressed as the mean ± SEM. Statistical differences were analyzed by unpaired two-sample Student's t test. p values <0.05 were considered as statistically significant.

SUPPLEMENTAL INFORMATION

Supplemental Information can be found online at https://doi.org/10.1016/j.ymthe.2020.12.025.

ACKNOWLEDGMENTS

This work was supported by the 2019 Post-Doc. Development Program of Pusan National University and the National Research Foundation (NRF) of Korea funded by the Korean government (MEST; 2018R1A2A3075038) to Y.J.

AUTHOR CONTRIBUTIONS

Y.J. conceived and designed the study. Y.S., J.K., C.L., M.K., J.H., and S.W. carried out experiments. Y.S., J.K., C.L., J.M.K., S.-C.S., B.-J.L., T.-J.K., and Y.J. interpreted the data. J.K. and Y.J. wrote the manuscript. Y.J. obtained funding. All authors approved the final version of the manuscript.

DECLARATION OF INTERESTS

The authors declare no competing interests.

REFERENCES

1. Bataller, R., and Brenner, D.A. (2005). Liver fibrosis. J. Clin. Invest. *115*, 209–218.
2. Pinzani, M., and Rombouts, K. (2004). Liver fibrosis: from the bench to clinical targets. Dig. Liver Dis. *36*, 231–242.
3. Alhadlaq, A., and Mao, J.J. (2004). Mesenchymal stem cells: isolation and therapeutics. Stem Cells Dev. *13*, 436–448.
4. Alfaifi, M., Eom, Y.W., Newsome, P.N., and Baik, S.K. (2018). Mesenchymal stromal cell therapy for liver diseases. J. Hepatol. *68*, 1272–1285.
5. Rong, X., Liu, J., Yao, X., Jiang, T., Wang, Y., and Xie, F. (2019). Human bone marrow mesenchymal stem cells-derived exosomes alleviate liver fibrosis through the Wnt/β-catenin pathway. Stem Cell Res. Ther. *10*, 98.
6. An, S.Y., Jang, Y.J., Lim, H.J., Han, J., Lee, J., Lee, G., Park, J.Y., Park, S.Y., Kim, J.H., Do, B.R., et al. (2017). Milk fat globule-EGF factor 8, secreted by mesenchymal stem cells, protects against liver fibrosis in mice. Gastroenterology *152*, 1174–1186.
7. Huang, B., Cheng, X., Wang, H., Huang, W., la Ga Hu, Z., Wang, D., Zhang, K., Zhang, H., Xue, Z., Da, Y., et al. (2016). Mesenchymal stem cells and their secreted molecules predominantly ameliorate fulminant hepatic failure and chronic liver fibrosis in mice respectively. J. Transl. Med. *14*, 45.

8. Berardis, S., Dwisthi Sattwika, P., Najimi, M., and Sokal, E.M. (2015). Use of mesenchymal stem cells to treat liver fibrosis: current situation and future prospects. World J. Gastroenterol. *21*, 742–758.

9. Volarevic, V., Nurkovic, J., Arsenijevic, N., and Stojkovic, M. (2014). Concise review: therapeutic potential of mesenchymal stem cells for the treatment of acute liver failure and cirrhosis. Stem Cells *32*, 2818–2823.

10. Eom, Y.W., Kim, G., and Baik, S.K. (2015). Mesenchymal stem cell therapy for cirrhosis: present and future perspectives. World J. Gastroenterol. *21*, 10253–10261.

11. Cho, K.A., Lee, H.J., Jeong, H., Kim, M., Jung, S.Y., Park, H.S., Ryu, K.H., Lee, S.J., Jeong, B., Lee, H., and Kim, H.S. (2019). Tonsil-derived stem cells as a new source of adult stem cells. World J. Stem Cells *11*, 506–518.

12. Ryu, K.H., Cho, K.A., Park, H.S., Kim, J.Y., Woo, S.Y., Jo, I., Choi, Y.H., Park, Y.M., Jung, S.C., Chung, S.M., et al. (2012). Tonsil-derived mesenchymal stromal cells: evaluation of biologic, immunologic and genetic factors for successful banking. Cytotherapy *14*, 1193–1202.

13. Park, G.C., Song, J.S., Park, H.Y., Shin, S.C., Jang, J.Y., Lee, J.C., Wang, S.G., Lee, B.J., and Jung, J.S. (2016). Role of fibroblast growth factor-5 on the proliferation of human tonsil-derived mesenchymal stem cells. Stem Cells Dev. *25*, 1149–1160.

14. Jung, N., Park, S., Choi, Y., Park, J.W., Hong, Y.B., Park, H.H., Yu, Y., Kwak, G., Kim, H.S., Ryu, K.H., et al. (2016). Tonsil-derived mesenchymal stem cells differentiate into a Schwann cell phenotype and promote peripheral nerve regeneration. Int. J. Mol. Sci. *17*, E1867.

15. Samivel, R., Kim, E.H., Chung, Y.J., and Mo, J.H. (2015). Immunomodulatory effect of tonsil-derived mesenchymal stem cells in a mouse model of allergic rhinitis. Am. J. Rhinol. Allergy *29*, 262–267.

16. Shin, S.C., Seo, Y., Park, H.Y., Jung, D.W., Shin, T.H., Son, H., Kim, Y.K., Lee, J.C., Sung, E.S., Jang, J.Y., et al. (2018). Regenerative potential of tonsil mesenchymal stem cells on surgical cutaneous defect. Cell Death Dis. *9*, 183.

17. Park, M., Kim, Y.H., Woo, S.Y., Lee, H.J., Yu, Y., Kim, H.S., Park, Y.S., Jo, I., Park, J.W., Jung, S.C., et al. (2015). Tonsil-derived mesenchymal stem cells ameliorate CCl_4-induced liver fibrosis in mice via autophagy activation. Sci. Rep. *5*, 8616.

18. Kim, Y.H., Cho, K.A., Park, M., Kim, H.S., Park, J.W., Woo, S.Y., and Ryu, K.H. (2018). Conditioned medium from tonsil-derived mesenchymal stem cells relieves CCl_4-induced liver fibrosis in mice. Tissue Eng. Regen. Med. *16*, 51–58.

19. Zhang, J., Li, S., Li, L., Li, M., Guo, C., Yao, J., and Mi, S. (2015). Exosome and exosomal microRNA: trafficking, sorting, and function. Genomics Proteomics Bioinformatics *13*, 17–24.

20. Witwer, K.W., Van Balkom, B.W.M., Bruno, S., Choo, A., Dominici, M., Gimona, M., Hill, A.F., De Kleijn, D., Koh, M., Lai, R.C., et al. (2019). Defining mesenchymal stromal cell (MSC)-derived small extracellular vesicles for therapeutic applications. J. Extracell. Vesicles *8*, 1609206.

21. Valadi, H., Ekström, K., Bossios, A., Sjöstrand, M., Lee, J.J., and Lötvall, J.O. (2007). Exosome-mediated transfer of mRNAs and microRNAs is a novel mechanism of genetic exchange between cells. Nat. Cell Biol. *9*, 654–659.

22. Phinney, D.G., and Pittenger, M.F. (2017). Concise review: MSC-derived exosomes for cell-free therapy. Stem Cells *35*, 851–858.

23. Keshtkar, S., Azarpira, N., and Ghahremani, M.H. (2018). Mesenchymal stem cell-derived extracellular vesicles: novel frontiers in regenerative medicine. Stem Cell Res. Ther. *9*, 63.

24. Bai, L., Shao, H., Wang, H., Zhang, Z., Su, C., Dong, L., Yu, B., Chen, X., Li, X., and Zhang, X. (2017). Effects of mesenchymal stem cell-derived exosomes on experimental autoimmune uveitis. Sci. Rep. *7*, 4323.

25. Hyun, J., Wang, S., Kim, J., Kim, G.J., and Jung, Y. (2015). MicroRNA125b-mediated Hedgehog signaling influences liver regeneration by chorionic plate-derived mesenchymal stem cells. Sci. Rep. *5*, 14135.

26. Feng, Y., Huang, W., Wani, M., Yu, X., and Ashraf, M. (2014). Ischemic preconditioning potentiates the protective effect of stem cells through secretion of exosomes by targeting Mecp2 via miR-22. PLoS ONE *9*, e88685.

27. Rockey, D.C., Housset, C.N., and Friedman, S.L. (1993). Activation-dependent contractility of rat hepatic lipocytes in culture and in vivo. J. Clin. Invest. *92*, 1795–1804.

28. Friedman, S.L. (2008). Hepatic stellate cells: protean, multifunctional, and enigmatic cells of the liver. Physiol. Rev. *88*, 125–172.

29. Cho, K.A., Park, M., Kim, Y.H., Woo, S.Y., and Ryu, K.H. (2017). RNA sequencing reveals a transcriptomic portrait of human mesenchymal stem cells from bone marrow, adipose tissue, and palatine tonsils. Sci. Rep. *7*, 17114.

30. Zhou, L., Liu, S., Han, M., Ma, Y., Feng, S., Zhao, J., Lu, H., Yuan, X., and Cheng, J. (2018). miR-185 inhibits fibrogenic activation of hepatic stellate cells and prevents liver fibrosis. Mol. Ther. Nucleic Acids *10*, 91–102.

31. Wang, Y., Du, J., Niu, X., Fu, N., Wang, R., Zhang, Y., Zhao, S., Sun, D., and Nan, Y. (2017). miR-130a-3p attenuates activation and induces apoptosis of hepatic stellate cells in nonalcoholic fibrosing steatohepatitis by directly targeting TGFBR1 and TGFBR2. Cell Death Dis. *8*, e2792.

32. Ji, X., Wu, B., Fan, J., Han, R., Luo, C., Wang, T., Yang, J., Han, L., Zhu, B., Wei, D., et al. (2015). The anti-fibrotic effects and mechanisms of microRNA-486-5p in pulmonary fibrosis. Sci. Rep. *5*, 14131.

33. Mastrolia, I., Foppiani, E.M., Murgia, A., Candini, O., Samarelli, A.V., Grisendi, G., Veronesi, E., Horwitz, E.M., and Dominici, M. (2019). Challenges in clinical development of mesenchymal stromal/stem cells: concise review. Stem Cells Transl. Med. *8*, 1135–1148.

34. Vizoso, F.J., Eiro, N., Cid, S., Schneider, J., and Perez-Fernandez, R. (2017). Mesenchymal stem cell secretome: toward cell-free therapeutic strategies in regenerative medicine. Int. J. Mol. Sci. *18*, E1852.

35. Ha, D., Yang, N., and Nadithe, V. (2016). Exosomes as therapeutic drug carriers and delivery vehicles across biological membranes: current perspectives and future challenges. Acta Pharm. Sin. B *6*, 287–296.

36. Yang, D., Zhang, W., Zhang, H., Zhang, F., Chen, L., Ma, L., Larcher, L.M., Chen, S., Liu, N., Zhao, Q., et al. (2020). Progress, opportunity, and perspective on exosome isolation - efforts for efficient exosome-based theranostics. Theranostics *10*, 3684–3707.

37. Théry, C., Amigorena, S., Raposo, G., and Clayton, A. (2006). Isolation and characterization of exosomes from cell culture supernatants and biological fluids. Curr. Protoc. Cell Biol. Chapter 3, Unit 3.22.

38. Soares Martins, T., Catita, J., Martins Rosa, I., A B da Cruz E Silva, O., and Henriques, A.G. (2018). Exosome isolation from distinct biofluids using precipitation and column-based approaches. PLoS ONE *13*, e0198820.

39. Božič, D., Sitar, S., Junkar, I., Štukelj, R., Pajnič, M., Žagar, E., Kralj-Iglič, V., and Kogej, K. (2019). Viscosity of plasma as a key factor in assessment of extracellular vesicles by light scattering. Cells *8*, E1046.

40. Kim, V.N. (2005). MicroRNA biogenesis: coordinated cropping and dicing. Nat. Rev. Mol. Cell Biol. *6*, 376–385.

41. Baglio, S.R., Rooijers, K., Koppers-Lalic, D., Verweij, F.J., Pérez Lanzón, M., Zini, N., Naaijkens, B., Perut, F., Niessen, H.W., Baldini, N., and Pegtel, D.M. (2015). Human bone marrow- and adipose-mesenchymal stem cells secrete exosomes enriched in distinctive miRNA and tRNA species. Stem Cell Res. Ther. *6*, 127.

42. Hyun, J., Wang, S., Kim, J., Rao, K.M., Park, S.Y., Chung, I., Ha, C.S., Kim, S.W., Yun, Y.H., and Jung, Y. (2016). MicroRNA-378 limits activation of hepatic stellate cells and liver fibrosis by suppressing Gli3 expression. Nat. Commun. *7*, 10993.

43. Wang, S., Kim, J., Lee, C., Oh, D., Han, J., Kim, T.J., Kim, S.W., Seo, Y.S., Oh, S.H., and Jung, Y. (2019). Tumor necrosis factor-inducible gene 6 reprograms hepatic stellate cells into stem-like cells, which ameliorates liver damage in mouse. Biomaterials *219*, 119375.